Biol. Cybern. 83, 461–470 (2000)

Biological Cybernetics

Investigations on emergent spatio-temporal neural response characteristics in a small network model

Ulrich Quill, Florentin Wörgötter

Institute of Physiology, Department of Neurophysiology, Ruhr-University Bochum, Germany

Received: 13 July 1999 / Accepted in revised form: 26 May 2000

Abstract. Although the functional role synchronous oscillations may play has been investigated in depth, the underlying processes and spatio-temporal aspects that establish the synchrony are still not thoroughly understood. Experimental studies suggest the existence of two types of activity: stimulus locked and stimulus induced. While stimulus-locked oscillations are systematically dependent on the stimulus (they are phase-locked to stimulus transients), stimulus-induced activity patterns (occurring in the γ-frequency range) show no such phase-locking. We propose a unifying approach which employs very generic connection structures. The above-mentioned two types of activity patterns with different temporal properties are observed as an emergent feature of the network structure. Our model demonstrates that stimulus-locked and stimulus-induced activity patterns are two distinct states of the same system. A transition from one state to the other is observed, and the influence of structural network parameters (e.g. connections strengths) on this behavior and its dependence on stimulus situations is investigated.

1 Introduction

Synchronization phenomena have long been an object of both experimental and theoretical research in the neurosciences. Although synchronous oscillations at different frequencies have been reported by various groups (Gray 1994; Singer and Gray 1995) Eckhorn et al. (1988a,b, 1991) were the first to introduce the terminology of two different kinds of neural response characteristics stimulus-locked and stimulus-induced activities. These activity patterns occur at different stages of the visual pathway (retina, LGN, cortex), but have also been observed in other parts of the brain, e.g. the auditory system (Steriade 1997).

Correspondence to: U. Quill
(Tel.: +49-234-7006955; Fax: +49-234-7004192
e-mail: quill@neurop2.ruhr-uni-bochum.de)

Stimulus-locked oscillations are directly driven by stimulus transients, to which they are phase-locked. Only strong transients, which occur for example during flashed stimuli, can elicit this type of oscillatory behavior (Wörgötter and Funke 1995; Funke and Wörgötter 1997).

Stimulus-induced activity patterns are supposed to be a results of self-organization processes among stimulus-driven "oscillators". Especially in the absence of strong stimulus transients, e.g. during slowly moving stimuli, these processes serve to generate synchronized response characteristics in the γ-frequency range.

We propose a simple, generic network model which is able to produce these two types of synchronous activity patterns with gradual transitions from one to the other. Thus, these different neuronal response types can be interpreted as two states of the same neural circuit, instead of being produced by different network types.

2 The model

Our model describes the information flow in the primary visual pathway. The afferent flow from LGN to cortical layers 4 and 6 is incorporated, as well as an excitatory feed-back loop from layer 6 to the LGN and an inhibitory feed-back loop from the perigeniculate nucleus (PGN) back to the LGN. The total cell number in the simulations ranged over about 800–2000 cells.

The basic simulator software has already been described by Wörgötter and Koch (1991) and Brettle and Niebur (1994). In our present model, we use an improved version which was presented by Köhn and Wörgötter (1996).

The retina is simulated as a simple preprocessing module for spike generation. Originally, this retina model consisted of ganglion cells represented by difference-of-Gaussian receptive field filters with spike generation by a stochastic process (Wörgötter and Koch 1991). As we focus primarily on the temporal characteristics of stimulus processing, it is not necessary to realistically model this step. Instead, we

resorted to directly calculate the retinal spike trains by mapping a Gaussian probability function. The standard deviation of the inter-spike interval distribution was 4 ms, and the mean value was contrast dependent. Thus, the mean firing frequency of the retinal ganglion cells directly reflects the intensity of the stimulus. This mean firing frequency was varied between 40 Hz (25-ms inter-spike interval mean, corresponding to 5% contrast) and 125 Hz (8 ms, corresponding to 100% contrast).

The dynamics of the improved integrate-and-fire neurons are described by the following differential equation for each cell i (Köhn and Wörgötter 1996):

$$C_i \frac{\mathrm{d}V_i}{\mathrm{d}t} = \sum_{j=1}^{k} g_{i,j,\mathrm{exc}}(t)(E_{\mathrm{exc}} - V_i) + \sum_{j=1}^{l} g_{i,j,\mathrm{inh}}(t)(E_{\mathrm{inh}} - V_i) + g_{\mathrm{leak}}(E_{\mathrm{leak}} - V_i) + g_{i,\mathrm{AHP}}(t)(E_{\mathrm{AHP}} - V_i) \ , \quad (1)$$

where C_i is the membrane capacity, V_i is the membrane potential, $g_{i,j,\mathrm{exc/inh}}(t)$ is the conductance of the excitatory/inhibitory channel from the presynaptic cell j at time t, g_{leak} is the leakage conductance, $g_{i,\mathrm{AHP}}(t)$ is the conductance of the after-hyperpolarization (AHP), $E_{\mathrm{exc/inh}}$ is the excitatory/inhibitory reversal potential, E_{leak} is the resting potential, and E_{AHP} is the reversal potential of the after-hyperpolarization (each of cell i). These differential equations are solved with a fourth-order Runge-Kutta method. The time courses of the conductances (excitatory, inhibitory, and after-hyperpolarization) are modeled by simple α-functions:

$$g_A = \hat{g}_A \frac{e}{\tau} t \mathrm{e}^{-t/\tau} \ ,$$

with $\hat{g}_A$ being the peak conductance, and τ being the time constant of channel A ($\tau = 1$ ms). For an overview of the parameter settings used in the simulations, see Table 1.

All computations were performed using discrete time steps of 0.1 ms. The spikes were generated by a simple thresholding mechanism, with $V_{\mathrm{threshold}} = -45$ mV for each cell. Spikes coming from any cell i are transmitted to a post-synaptic cell j with a synaptic delay d_{ij}. Computationally, this means that in the specific postsynaptic cell j, a postsynaptic potential (described by the α-functions) is generated d_{ij} ms after a spike is emitted by presynaptic cell i. The convolutions of the input functions for each cell (a sequence of spikes) were solved using the Z-transform method (Köhn and Wörgötter 1998).

Table 1. Main parameter settings used in the simulations

Value	Parameter	Value
C	Capacity	1 nF for LGN and 2 nF for cortex
G_{leak}	Leakage conductance	0.1 μS for LGN and 0.2 μS for cortex
E_{leak}	Leakage reversal potential	−71 mV
τ_{AHP}	Time constant of AHP	1 ms
E_{AHP}	Reversal potential of AHP	−91 mV
g_{AHP}	Peak conductance of AHP	0.59 μS
w_{AHP}	Synaptic weight of AHP	50

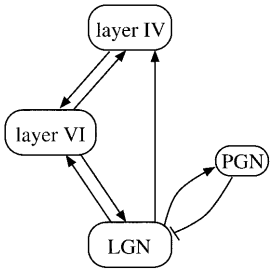

Fig. 1. General connection structures between principal neuronal layers

The network consists of two general types of neurons: thalamic and cortical. The primary connections between these functional layers are shown in Fig. 1.

LGN and cortical layer 4 cells are topographically arranged on a rectangular grid. For simplicity, we only used ON-type LGN cells. These cells are excitatorily connected with both types of cortical cells (layers 4 and 6). The thalamo-cortical connections are topographically arranged with Hubel-Wiesel-type receptive fields (RFs) for both the layer-4 and layer-6 neurons (Hubel and Wiesel 1962; Jones and Palmer 1987). As our model is primarily aimed at demonstrating and examining synchronization phenomena, we confined ourselves to receptive fields comprized of simple precisely tuned feed-forward LGN-cortex structures, and did not incorporate more realistic models of orientation specificity (as did, e.g. Wörgötter and Koch 1991; Somers et al. 1995). A grid of $a_i \times b_i$ LGN cells projects onto each cortical layer 4 cell i. The weights of these feed-forward connections are expressed by Gaussians of the following form:

$$W_{j \to i} = W_{j \to i,0} \exp\left[-\frac{(x_j - x_i)^2}{2\sigma_{i,x}^2} \right] \exp\left[-\frac{(y_j - y_i)^2}{2\sigma_{i,y}^2} \right] \ . \quad (2)$$

For the sake of simplicity, we assume that the receptive field is oriented to 90°, so that a_i is the number of cells in the x-direction, b_i is the number of cells in the y-direction. Other orientations only result in appropriate coordinate transforms. $x_{i,j}, y_{i,j}$ are the coordinates of cell i (CTX) and j (LGN) on the grid, and $W_{j \to i,0}$ is the maximal weight reached in the RF center. The parameters $\sigma_{x/y}$ are chosen in such a way that the weight decays to $W_{j \to i,0}\mathrm{e}^{-1}$ at the border of the receptive field in both directions, the preferred orientation and the orthogonal direction:

$$\exp\left[-\frac{(a/2)^2}{2\sigma_{i,x}^2} \right] = \mathrm{e}^{-1} \quad \text{and} \quad \exp\left[-\frac{(b/2)^2}{2\sigma_{i,y}^2} \right] = \mathrm{e}^{-1} \ , \quad (3)$$

which leads to

$$\sigma_{i,x} = \frac{a_i}{4}\sqrt{2} \quad \text{and} \quad \sigma_{i,y} = \frac{b_i}{4}\sqrt{2} \ .$$

In our simulations the number of LGN cells converging on a cortical layer 4 neuron ranged over about 5–30

Table 2. Variability of some decisive neuronal parameters. Within one simulation run the parameters varied with a Gaussian distribution with the above values for mean (w_0, d_0) and standard deviation (σ)

Connection	Connection strength	Delay (ms)
LGN → CTX4	$w_0 = 10, \sigma = 2$	$d_0 = 4, \sigma = 2$
LGN → PGN	$w_0 = 6, \sigma = 2$	$d_0 = 2, \sigma = 1$
PGN → LGN	$w_0 = 5, \sigma = 2$	$d_0 = 2, \sigma = 1$
CTX4 → CTX6	$w_0 = 4, \sigma = 2$	$d_0 = 2, \sigma = 2$
CTX6 → CTX4	$w_0 = 4, \sigma = 2$	$d_0 = 2, \sigma = 2$
LGN → CTX6	$w_0 = 4, \sigma = 2$	$d_0 = 8, \sigma = 1.5$
CTX6 → LGN	$w_0 = 4, \sigma = 2$	$d_0 = 10, \sigma = 1.5$

with RF aspect ratios between 1:5 and 3:10, with an average of 1:4. The time delays of the connections were also set in a similar (i.e. Gaussian) distribution, with the delays increasing towards the edges of the receptive fields. This delay distribution is in accordance with biological findings, e.g. Bringuier et al. (1999). For an overview of the parameter settings, see Table 2. The values of the delays depicted there are the maximum values from one RF and their variations across different cells (within one simulation run). These afferent LGN-layer-4 connections are fast and strong and act as the primary, stimulus-dependent driving force of the layer 4 neurons.

Layer 6 neurons also obtain input from the LGN. Their receptive fields are also described by a Gaussian weight distribution (see Eq. 3), but are broader than those of layer 4 neurons (Humphrey et al. 1985; see also Sect. 3.1). There are two types of efferent connections from these layer 6 neurons; firstly, divergent feed-forward projections onto layer 4 with adjustable divergence parameters and, secondly, feed-back projections to the LGN with a point-spread function (PSF) broader than the respective feed-forward RF. Here, the RF aspect ratios ranged around 1:2 with about 10–45 LGN cells converging onto a layer 6 cell. The PSF from one layer 6 neuron to layer 4 usually covered 5–10 layer 4 cells. Both the RF and the PSF connection weights are distributed in a Gaussian fashion (see Eq. 3). The connection structures involving the layer 6 neurons perform two tasks. First, the neurons can reflect tonic firing patterns from the LGN and maintain these patterns for some time, even if LGN firing ceases. Furthermore, the broader convergence and divergence of their connections helps to spread activity across adjacent neurons (both in the LGN and cortical layer 4).

Finally, there is the LGN-PGN feed-back loop with excitatory feed-forward and inhibitory feed-back connections, both with a rather circular shaped RF and PSF. We chose radii of about 2–4 LGN cells for the RFs and 3–6 LGN cells for the backprojecting connections. This loop is an oscillator with alternating states and thus modulates the LGN activity with its resonance frequency. The existence of this kind of inverse correlation between LGN and PGN cells and how it corresponds to different system states (e.g. drowsy versus awake) was shown by Funke and Eysel (1998, 2000; see also Sect. 3).

The cells in the different layers are arranged in topography preserving grid structure. Both types of cortical neurons are located above the LGN cell at the center of their respective RFs. The feed-forward connections from layer 6 to layer 4 always cover adjacent neurons, thus ensuring an integration over overlapping (LGN to layer 4) RFs.

In our experiments, we used two general types of stimuli; flashed and moving light bars. These covered about $2^\circ \times 2^\circ$ to $4^\circ \times 4^\circ$ of the visual field. Presentation time for the flashed bars was 700 ms. The intensities of the bars were varied in front of a constant dark background. In this study, "input frequency" always means the coding frequency corresponding to a certain stimulus, i.e. the mean firing rate of the retinal ganglion cells. In the motion experiments, different velocities as well as different intensities were used.

Throughout this paper, we usually show and analyze cortical local field potentials (LFPs) and/or multi-unit activity (MUA). The first is calculated in the simulator software by averaging over the membrane potentials, which is a sufficient approximation to biologically recorded field potentials:

$$V_{\mathrm{LFP}}(t) = \frac{1}{N}\sum_{i=1}^{N} V_i(t), \quad \text{with } N = \text{number of cells} \ .$$

The MUAs are usually shown for bin widths of 1 ms and are calculated in the same way as peri-stimulus time histograms (PSTHs). Analysis was usually done in the frequency domain by calculating the power spectra of the LFP or MUA signals using standard software techniques (Press et al. 1992).

3 Results

3.1 Flashed stimuli

The first experiments were carried out with bar stimuli. A light bar on a dark background was switched on for about 700 ms. The intensity of the bar was changed in different experiments to analyze the behavior of the system in the presence of different retinal ganglion cell firing frequencies. In these experiments with only the LGN-CTX4 connection present, two domains can be observed in the response of the cortical cells in layer 4 (Fig. 2). Immediately after stimulus onset, an undisturbed oscillation can be seen, which lasts for about 70–100 ms, and which shows the same frequency as the firing of retinal ganglion cells which, in turn, reflects the intensity of the stimulus. After this fast stimulus-locked component, the cortical cells maintain a rather indifferent state for the remaining stimulus presentation time. During this state, no distinct frequency component is observed. In Fig. 2, this behavior is demonstrated by an LFP as well as an MUA plot (inset). The power spectrum also shows that there is only a frequency component of 100 Hz, corresponding to the firing rate of retinal ganglion cells.

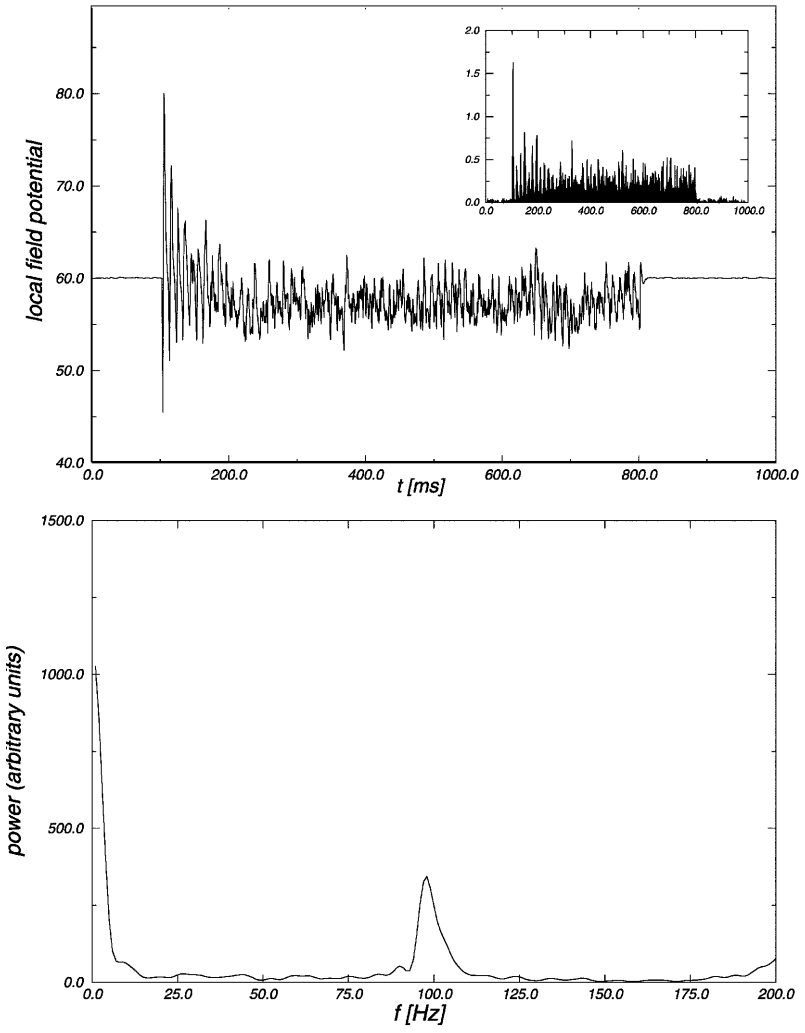

Fig. 2. Illustration of a general cortical local field potential and the corresponding power spectrum, with only the LGN-CTX4 connections being present, so that an initial presynchronization of the LGN cells is the only possible driving force for a stimulus-locked component. This component of around 100 Hz can be seen in the LFP of about 100–200 ms (the retinal ganglion cells' firing frequency was 100 Hz). *Top panel*: the cortical local field potentials (LFP) (*inset* shows the corresponding multi unit activity peak stimulus time histogram). *Bottom panel*: power spectrum of the LFP

These two response domains were further investigated. We observed that the stimulus-locked component occurs with only the feed-forward connections from LGN being in effect. The connection strength only modulates the "strength" of the component, i.e. it determines whether or not the component can be seen in the cortical LFPs and the amplitude of the oscillations. This led to the conclusion that this stimulus-locking is an effect dominated solely by the properties of the LGN answers. Indeed, the reason for LFP oscillations is a presynchronization of LGN neurons. When the stimulus is switched on, nearly all LGN neurons covered by it start firing in a state of phase-locking (Wörgötter and Funke 1995). Due to overlapping receptive fields, this phase-locking is transmitted without much jitter to the CTX4 cells. This results in the observed stimulus-locked oscillations at the beginning of the LFP plots. The time scale is dependent on the duration of the phase-locking of the LGN neurons. Figure 3 shows how the behavior of the locked component depends on the degree of LGN presynchronization. Coincidence plots for the LGN neurons were calculated by counting all the spikes of the associated population within a given time window (here: 5 ms) and dividing this by the total number of cells. The figure shows that, with the synchronization index diminishing both in strength and duration (left column), the stimulus-locked component the LFP plots also diminishes (right column).

In these flashed bar simulations, only those LGN cells which were ideally stimulated by the bar were taken into account. Therefore, all the LGN cells fire at the same frequency. In a typical experimental situation, this would, of course, not be the case. Due to a different overlap of the stimulus and the receptive fields of LGN neurons, there would be a broader spread in the frequency distribution of the firing pattern of LGN cells. This would also result in a decay of both strength and duration of the stimulus-locked component, because an initially broader frequency distribution of LGN cells already implies a lower presynchronization than in the case of nearly the same firing frequency. To further illustrate this effect, simulations with broader frequency distributions were carried out. Figure 4 shows the results comparing the optimal and the non-optimal situation. The top three panels show a stimulus situation comparable to that of Fig. 2. The LGN neurons were stimulated with a narrow frequency distribution around 100 Hz, pro-

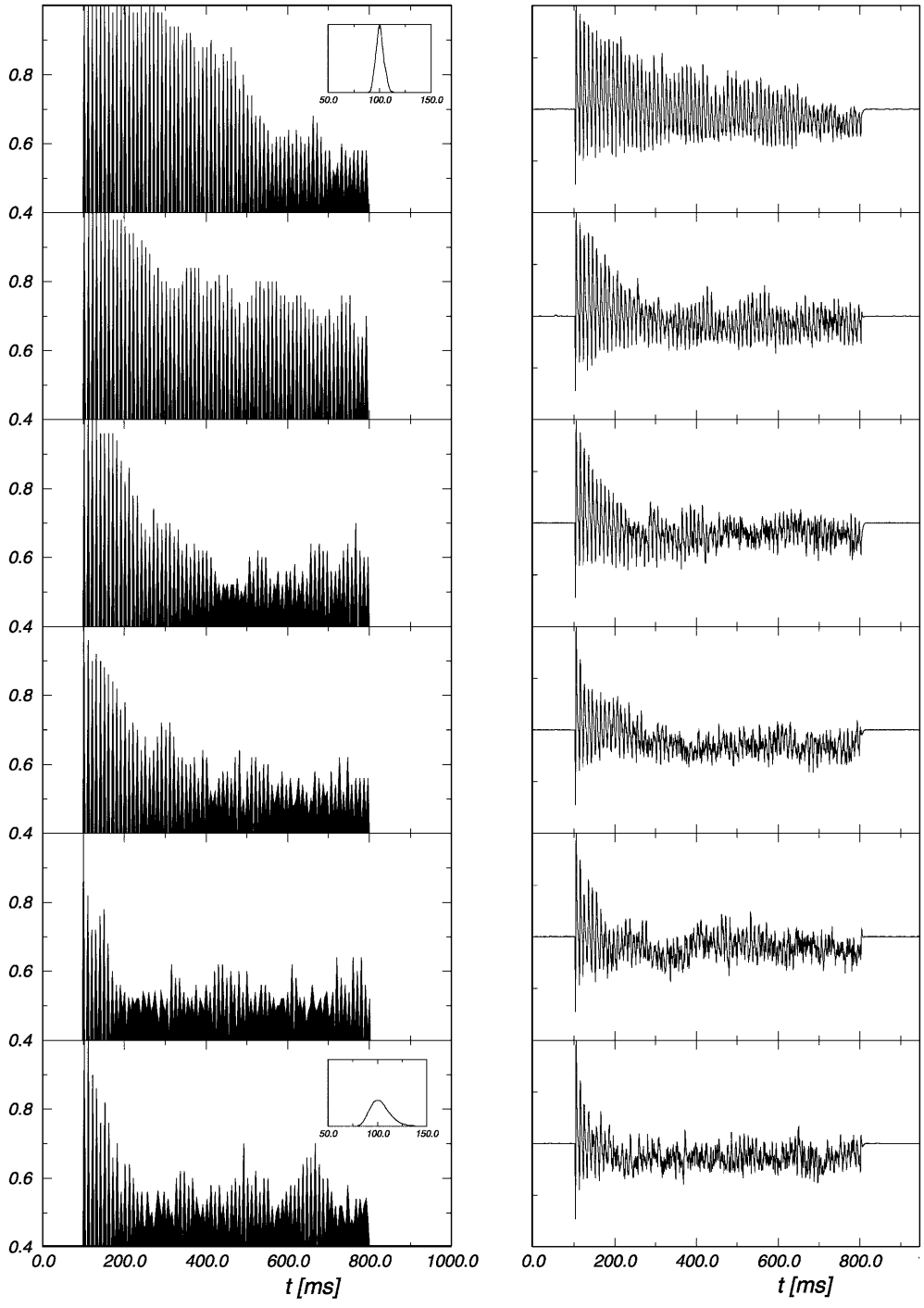

Fig. 3. Influence of LGN cell presynchronization on the stimulus-locked component in the cortical answers. *Left column*: LGN cell coincidence plots. These plots are calculated by counting all the spikes of the cell population within a given time window and dividing this by the total number of cells, thus 1.0 means fully coincident firing of all cells. The *y*-axis starts at 0.4, and the window width was chosen as 5 ms. By changing the input to the LGN cells in strength and coincidence, the presynchronization of the LGN cells was modified; it diminishes from top to bottom. Other network parameters were kept constant. The insets in the first and last coincidence plots show the firing frequency distribution of the LGN cells. *Right column*: cortical local field potentials (LFPs) for the corresponding presynchrony of LGN cells

ducing the stimulus-locked component. In the bottom panels, the results for a broader frequency distribution (again around 100 Hz, corresponding to the 10-ms inter-spike-interval) are presented, showing that, in this case, the stimulus-locked pattern vanishes. As explained above, this effect can be interpreted as resulting from the loss in synchrony among the LGN neurons. Experimental results, however, show that flashing bar stimuli can indeed lead to a high level of synchrony in the LGN (Wörgötter and Funke 1995). As a consequence, the situation shown in Fig. 2 is probably still rather close to reality. In contrast, the situation depicted in the three bottom panels of Fig. 4 more closely resembles a stimulus such as a moving bar, where there is no strong stimulus-locked synchronization.

When all the connections shown in Fig. 1 are active, a slightly different result can be observed in the flashed bar experiments (see Fig. 5). The stimulus-locked component still exists, but now the later domain in the cortical layer 4 responses is governed by a different behavior. The cortical cells fire synchronously with a characteristic frequency. This frequency does not directly depend on the input frequency anymore. Instead, the properties of

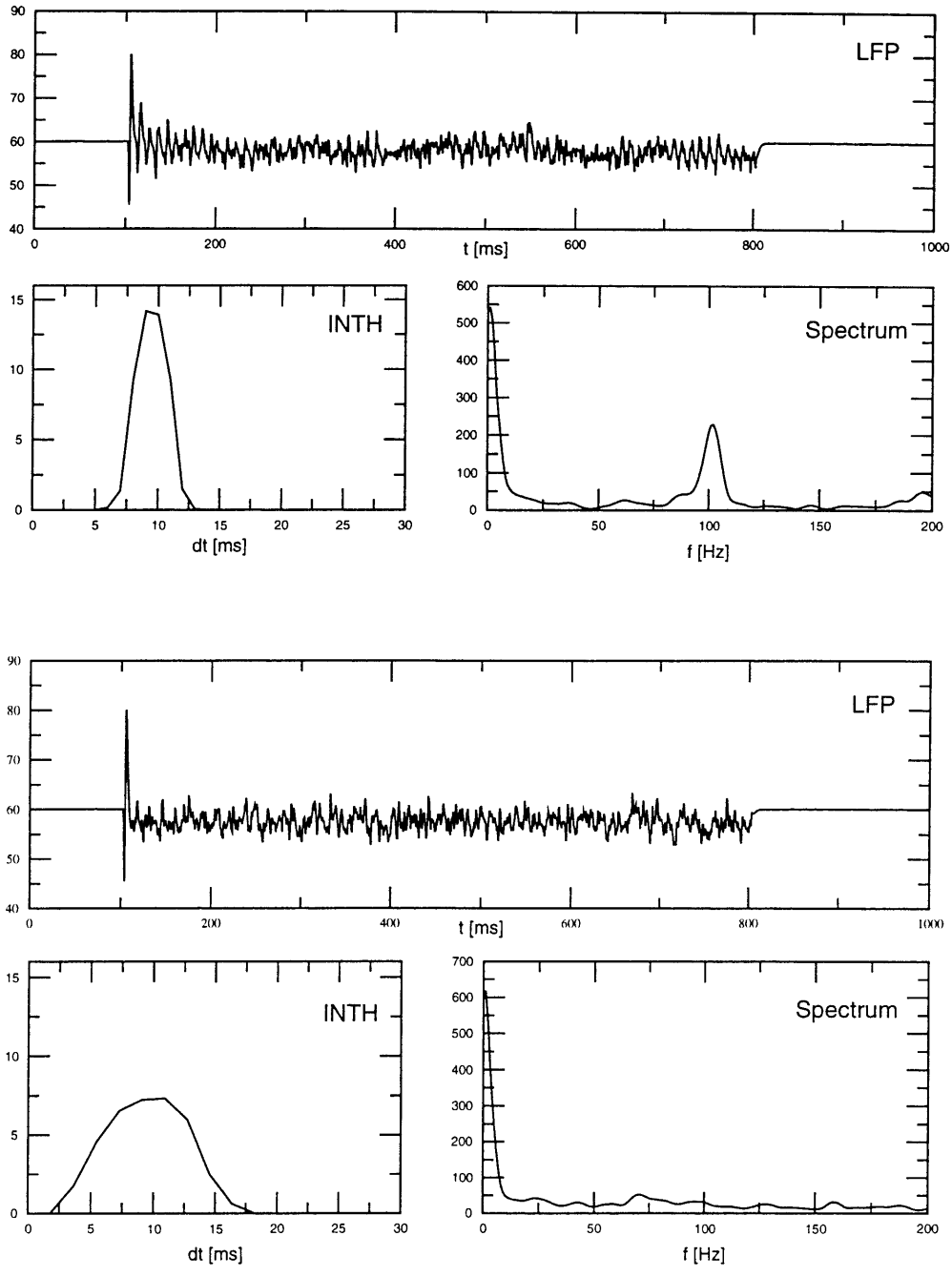

Fig. 4. Broader frequency distributions in the LGN destroy the stimulus-locked activity patterns. *Top three panels*: local field potential (LFP), inter-spike-interval histogram (INTH) and power spectrum (spectrum) for the optimal stimulus situation (narrow LGN stimulation around 100 Hz $\equiv$ 10 ms inter-spike-interval). The stimulus-locked component can be observed immediately after 100 ms in the LFP plot and is also reflected in the power spectrum (peak at 100 Hz). *Bottom*: local field potential (LFP), inter-spike-interval histogram (INTH) and power spectrum (spectrum) for the non-optimal stimulus situation (broader LGN stimulation around 100 Hz). The stimulus-locked component has now vanished (both in the LFP plot, and the power spectrum)

this stimulus-induced component are influenced by the properties of the LGN-CTX4-CTX6 loop. This behavior is documented in the MUA plot (Fig. 5, large plot), where the locked component is present at about 100–200 ms and the induced component becomes predominant after about 240 ms. These components can also be identified in the power spectrum (Fig. 5, inset). Peak 1 at 57 Hz is the locked component, peak 2 at 80 Hz is the frequency induced by the network, and peak 3 at 160 Hz is its first harmonic.

The neuronal structures in cortical layer 6 are excited by the LGN neurons and start to fire with characteristic frequencies. These characteristic frequencies do not directly reflect the input frequency. Instead, they are dependent on the structural and cell parameters (connection strength, synaptic delays and intrinsic parameters of the cells; see Fig. 6 for a qualitative overview). The cells in layer 6 have broader receptive fields as those in layer 4, and they also produce a broader point-spread function. Thus, even less excitation of LGN neurons can still excite the layer 6 neurons strongly and establish a prominent stimulus-induced component in the answer of layer 4 neurons. Figure 7 shows an example of this behavior. During the active periods of the PGN, the LGN-CTX4-CTX6 pathway is still strong enough to establish and maintain the stimulus-induced activity. The stimulus-locked component, though, has nearly vanished. The beginning of stimulation is coincident with an active period of the PGN, and thus the initial presynchronization of LGN neurons is weakened

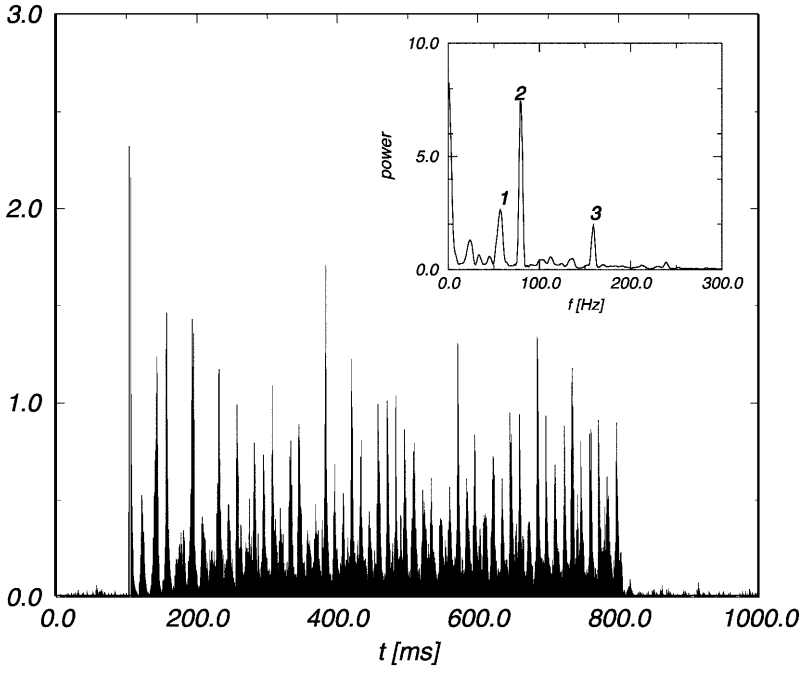

Fig. 5. Illustration of both activity patterns observed in the cortical responses. *Large*: multi-unit activity of cortical neurons. At 100–200 ms, there is the slower stimulus-locked component, after which the faster, induced component is maintained. *Small*: corresponding frequency analysis. The retinal ganglion cell firing frequency was 57 Hz (*peak 1*). The frequency induced by the network structure is 80 Hz (*peak 2*). *Peak 3*, at 160 Hz, is just the double frequency of the 80-Hz component and, as such, is an artifact of the spectral analysis. The double frequency of the 57-Hz component is so small that it is nearly invisible (small bulge before peak 3)

so much that the component is nearly invisible in the MUA. Only the frequency analysis shows that the input frequency is still present in the neuronal answer (see Fig. 7, bottom).

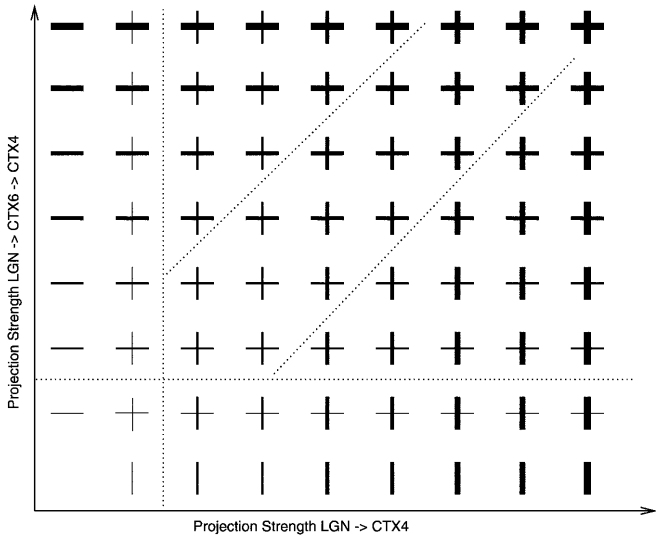

Fig. 6. A qualitative diagram showing the dependency of the stimulus-locked and stimulus-induced components on the connections strengths to cortical layers 4 and 6 (both axes in arbitrary units). The strength of the stimulus-locked component is coded by *vertical lines*, that of the stimulus-induced component by *horizontal lines*, with *thick lines* meaning a strong component. These strengths correspond to the peak value of the normalized power spectrum at the respective frequency. Generally, there is a smooth transition in the response characteristics, but some domains can roughly be identified, corresponding to the regimes: no distinct response, one of the two components dominates, both components are equally present. Approximate boundaries of these domains are indicated by *dotted lines* in the diagram

3.2 Slowly moving stimuli

Experimental studies have shown that, in the case where slowly moving bars were presented as stimuli, no stimulus-locked components could be observed (Kruse 1993).

In order to show that our model also produces the results found in these experiments, slowly moving bars with different velocities and contrasts were presented. Figure 8 shows some typical results. The model produces no stimulus-locked component for the given stimulus paradigm. The non-phase locked oscillations are observed for velocities starting at about 5 deg/s. The results in Fig. 8 were obtained around this transitional velocity. The graph at the top shows the results for a stimulus velocity of around 5.8 deg/s, whereas at the bottom, the results for a stimulus velocity of about 3 deg/s are shown.

The reason for this is evident. In the case of slowly moving bars, the presynchronization of the LGN cells is very low, because the receptive fields of the retinal ganglion cells are not ideally stimulated all at the same time. The excitation slowly builds up when the stimulus enters the receptive field, then decays again when the stimulus leaves the RF. This pattern of excitation is then also taken up by the LGN cells. However, the presynchronization in the LGN is the dominating factor for the emergence of stimulus-locked components. Without the presynchronization, no such components can occur.

Stimulus-induced components can still be observed. These components are dominated by the LGN-CTX6-CTX4 loop and are independent of the presynchronization of the LGN cells. Nevertheless, due to the longer time scale on which this loop takes effect, the stimulus-induced components can only be observed in the situation of very slow bar movements (see Fig. 8).

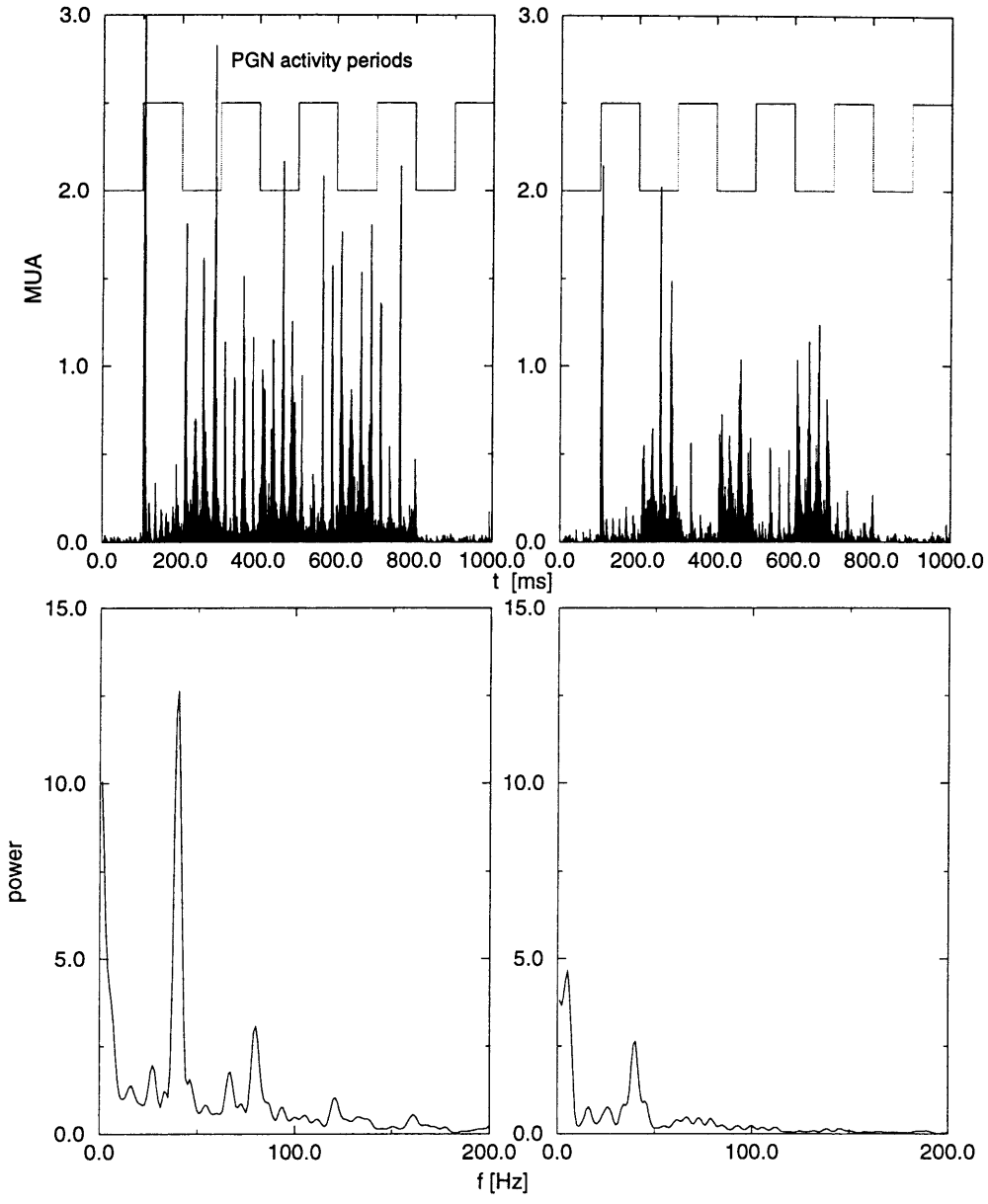

Fig. 7. An example of how the intrinsic LGN-CTX4-CTX6 structures are able to establish and maintain a stimulus-induced activity even with reduced LGN activity. *Above*: multi-unit activity of layer 4 neurons. Also shown are the periods of perigeniculate nucleus (PGN) activity and inactivity. *Below*: the power-spectrum of the multi-unit activity (MUA). The retinal ganglion cell firing frequency (stimulus) was 80 Hz, the intrinsic (induced) frequency was 40 Hz

4 Discussion

We could show that a very simple yet biologically plausible model of the primary visual pathway is able to establish two patterns of neuronal activity; stimulus-locked and stimulus-induced, both of which have been found in biological experiments (Eckhorn et al. 1988a,b; Tallon-Baudry et al. 1996). These patterns emerge within one network in the form of a transition from one to the other.

Currently, our model was chosen to be as simplistic as possible while still maintaining biological plausibility. In this respect, improved integrate-and-fire neurons were employed, but cell numbers were kept small. The LGN-PGN inhibitory loop was incorporated as the only specific local circuitry to model the antagonistic response characteristics of topographically matched LGN and PGN cells (Funke and Eysel 1998). The next extension will thus be targeted towards greater realism regarding the size of the model (see, e.g. Lumer et al. 1997 for a large scale model). This will also enable us to enhance the quantitative accordance with biological findings, especially with respect to the frequency ranges and exact time scales of the observed modes. Although some correspondence already emerged (compare, e.g. the 50-Hz peak of Fig. 8 with Kruse 1993), we focused primarily on the "proof-of-existence" approach by demonstrating the qualitative existence of the effects. We suppose, though, that the biological match will not be difficult, because the observed results are already within the correct order of magnitude (see Sect. 3, and, e.g. Kruse 1993; Eckhorn et al. 1988a,b; Eckhorn 1991). Additionally, quantitative deviations may also result from other simplifications made in our model, such as, e.g. rather straightforward orientation specificity. More detailed models (Somers et al. 1995), which incorporate a

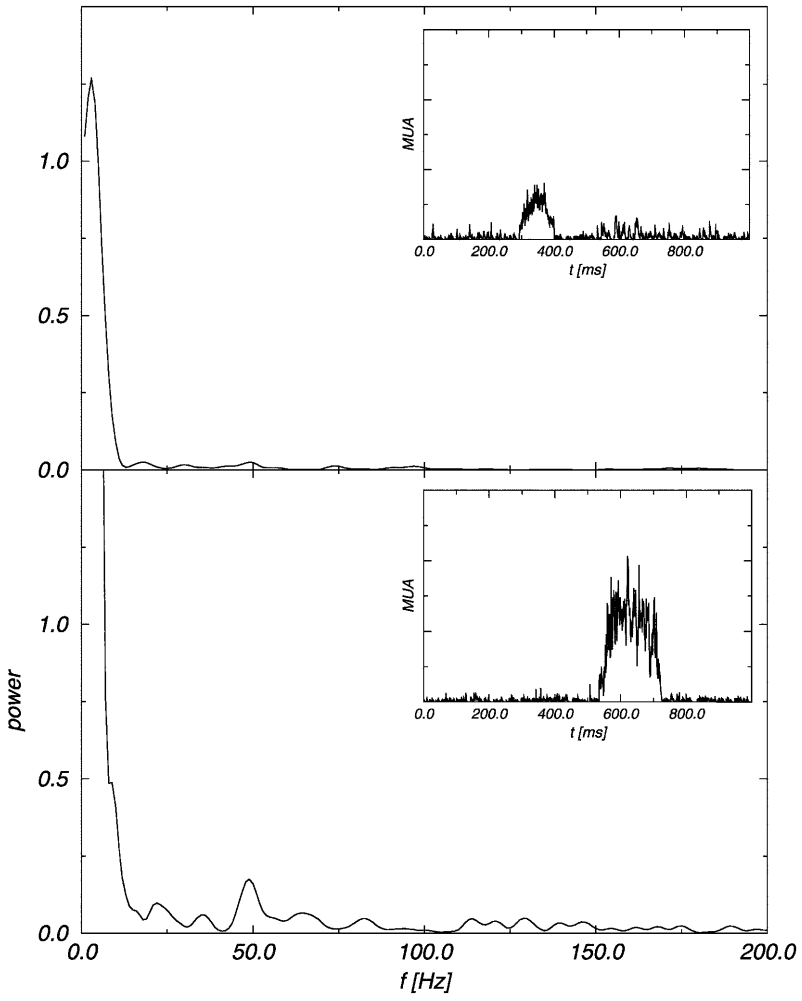

Fig. 8. Power spectra (*large plots*) and local field potential (LFP) plots (*inlays*) for moving stimuli. Both plots were obtained for medium contrast stimuli. *Top*: power spectrum for fast stimulus movement (bar velocity $\approx$ 5.8 deg/s), *inset* shows the multi-unit activity (MUA). *Bottom*: power spectrum and MUA for slow movement (velocity $\approx$ 3 deg/s). An oscillation around 50 Hz can be observed

higher degree of interconnectivity among the neurons, can very well lead to different results in timing and oscillation frequencies.

Other more abstract models have been suggested to explain the non-phase locked oscillations (e.g. Deppisch et al. 1994). These models deliver a formal description for the underlying system states which reproduces experimental results (e.g. hidden Markov systems), but they do not describe the connectivity of the system. In contrast, our model is built in a bottom-up fashion, paying much attention to the network structure, while it does not try to find a formal description of the system in a closed form.

A functional significance of the described mechanisms could be seen in different cognitive stages. The transition from very fast stimulus-locked synchronizations to slower but longer lasting stimulus-induced activity may be related to a coarse-to-fine recognition process, where simple tasks are solved on a short timescale (Thorpe et al. 1996), followed by a slower processing stage used for thorougher evaluation of a visual scene.

Furthermore, this behavior may also be correlated to mechanisms of visual attention. The antagonistic LGN-PGN response characteristics are correlated to EEG activity patterns (Funke and Eysel 1998). During an EEG delta wave regimen (corresponding to sleepiness), a high PGN activity and a low LGN activity was observed, and during an aroused state, this situation was inverted. We could show (Fig. 7) that, during strong PGN activity, nearly no stimulus-induced activity is maintained. Only a strong transient at stimulus onset can be registered. During periods of low PGN activity, the induced component can be observed. Therefore, our model supports the idea that during a sleepy state only strong stimulus transients will be recognized (''wake-up signal'') whereas, in an aroused state, the induced activity can be maintained (''scene evaluation'').

Acknowledgments. The authors would like to thank K. Funke for valuable discussions on the manuscript. This study was supported by the Deutsche Forschungsgemeinschaft (SFB 509) and the HFSP.

References

Brettle D, Niebur E (1994) Detailed parallel simulation of a biological neuronal network. IEEE Comp Sci Eng 1(4): 31–43

Bringuier V, Chavane F, Glaeser L, Frégnac V (1999) Horizontal propagation of visual activity in the synaptic integration field of area 17 neurons. Science 283: 695–699

Deppisch J, Pawelzik K, Geisel T (1994) Uncovering the synchronization dynamics from correlated neuronal activity quantifies assembly formation. Biol Cybern 71: 387–399

Eckhorn R (1991) Stimulus-specific synchronizations in the visual cortex: linking of local features into global figures? In: Krüger J (ed) Neuronal Cooperativity. Springer Series in Synergetics, vol 49, chap 9. Springer, Berlin Heidelberg New York

Eckhorn R, Bauer R, Jordan W, Brosch M, Kruse W, Munk M, Reitboeck H (1988a) Coherent oscillations: a mechanism of feature linking in the visual cortex? multiple electrode and correlation analysis in the cat. Biol Cybern 60: 121–130

Eckhorn R, Reitboeck H, Arndt M, Dicke P (1988b) Feature linking via stimulus-evoked oscillations: experimental results from cat visual cortex and functional implications from a network model. Proc Int Joint Conf Neural Networks I: 723–730

Eckhorn R, Reitboeck H, Arndt M, Dicke P (1990) Feature linking via synchronization among distributed assemblies: simulations of results from cat visual cortex. Neural Comp 2: 293–307

Funke K, Wörgötter F (1995) Temporal structure in the light response of relay cells in the dorsal lateral geniculate nucleus of the cat. J Physiol 485: 715–737

Funke K, Wörgötter F (1997) On the significance of temporally structured activity in the dorsal lateral geniculate nucleus (lgn). Prog Neurobiol 53: 67–119

Funke K, Eysel UT (1998) Inverse correlation of firing patterns of single topographically matched perigeniculate neurons and cat dorsal lateral geniculate relay cells. Visual Neurosci 15: 1–19

Funke K, Eysel UT (2000) Quantitative aspects of the state-dependent co-variation of cat lateral geniculate and perigeniculate visual activity. Neuroreport 11: 1031–1037

Gray C (1994) Synchronous oscillations in neuronal systems: mechanisms and functions. J Comp Neurosci 1: 11–38

Hubel D, Wiesel T (1962) Receptive fields, binocular interaction and functional architecture in the cat's visual cortex. J Physiol 160: 106–154

Humphrey A, Sur M, Uhlrich D, Sherman S (1985) Projection patterns of individual x- and y-cell axons from the lateral geniculate nucleus to cortical area 17 in the cat. J Comp Neurol 233: 159–189

Jones J, Palmer L (1987) The two-dimensional spatial structure of simple receptive fields in cat striate cortex. J Neurophysiol 58: 1187–1211

Köhn J, Wörgötter F (1996) Cortifugal feedback can reduce the visual latency of responses to antagonistic stimuli. Biol Cybern 75: 199–209

Köhn J, Wörgötter F (1998) Employing the z-transform to optimize the calculation of the synaptic conductance of nmda and other synaptic channels in network simulations. Neural Comp 10: 1639–1651

Kruse W (1993) Zwei Arten reizspezifischer Synchronisation im visuellen Kortex. PhD thesis. Phillipps-Universität Marburg, Germany

Lumer E, Edelman G, Tononi G (1997) Neural dynamics in a model of the thalamocortical system. i. layers, loops and the emergence of fast synchronous rhythms. Cerebral Cortex 7: 207–227

Press WH, Teukolsky SA, Vetterling WT, Flannery BP (1992) Numerical recipes in C – the art of scientific computing. Cambridge University Press, Cambridge

Singer W, Gray C (1995) Visual feature integration and the temporal correlation hypotheses. Ann Rev Neurosci 18: 555–586

Somers DC, Nelson SB, Sur M (1995) An emergent model of orientation selectivity in cat visual cortical simple cells. J Neurosci 15: 5448–5465

Steriade M (1997) Synchronized activities of coupled oscillators in the cerebral cortex and thalamus at different levels of vigilance. Cerebral Cortex 7: 583–604

Tallon-Baudry C, Bertrand O, Delpuech C, Pernier J (1996) Stimulus specificity of phase-locked and non-phase-locked 40 Hz responses in human. J Neurosci 16: 4240–4249

Thorpe S, Fize D, Marlot C (1996) Speed of processing in the human visual system. Nature 381: 520–522

Wörgötter F, Koch C (1991) A detailed model of the primary visual pathway in the cat: comparison of afferent excitatory and intracortical inhibitory connection schemes for orientation selectivity. J Neurosci 11: 1959–1979

Wörgötter F, Funke K (1995) Fine structure analysis of temporal patterns in the light response of cells in the lateral geniculate nucleus of cat. Vis Neurosci 12: 469–484